ACS APPLIED MATERIALS & INTERFACES

Letter

www.acsami.org

Building High-Efficiency CdS/CdSe-Sensitized Solar Cells with a Hierarchically Branched Double-Layer Architecture

Zonglong Zhu, Jianhang Qiu, Keyou Yan, and Shihe Yang*

Nano Science and Technology Program, Department of Chemistry, The Hong Kong University of Science and Technology, Clear Water Bay, Kowloon, Hong Kong

Supporting Information

ABSTRACT: We report a double-layer architecture for a photoanode of quantum-dot-sensitized solar cells (QDSSCs), which consists of a ZnO nanorod array (NR) underlayer and a ZnO nanotetrapod (TP) top layer. Such double-layer and branching strategies have significantly increased the power conversion efficiency (PCE) to as high as 5.24%, nearly reaching the record PCE of QDSSCs based on TiO_2. Our systematic studies have shown that the double-layer strategy could significantly reduce charge recombination at the interface between the charge collection anode (FTO) and ZnO nanostructure because of the strong and compact adhesion of the NRs and enhance charge transport due to the partially interpenetrating contact between the NR and TP layers, leading to improved open-circuit voltage (V_{oc}) and short-circuit current density (J_{sc}). Also, when the double layer was subjected to further branching, a large increase in J_{sc} and, to a lesser extent, the fill factor (FF) has resulted from increases in quantum-dot loading, enhanced light scattering, and reduced series resistance.

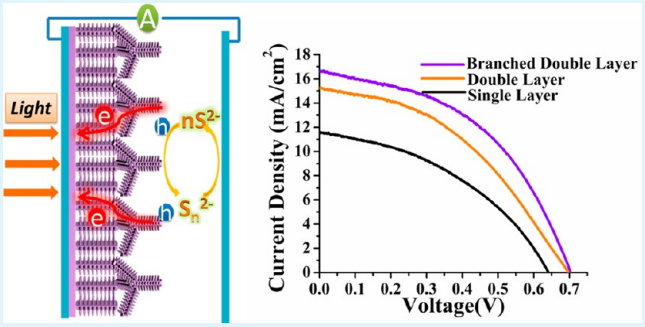

KEYWORDS: *high-efficiency semiconductor-sensitized solar cells, branched double-layer photoanode, suppressed recombination, improved charge transport*

Over the past few years, quantum-dot-sensitized solar cells (QDSSCs) have progressed considerably as a promising type of new generation photovoltaic devices.[1−4] QDSSC has its root in dye-sensitized solar cells (DSSCs) differing only by replacing the dye with narrow-band-gap semiconductor nanocrystals such as CdS,[5−7] CdSe,[8−10] PbS,[11−13] SnS_2,[14] etc., anchored on a wide-band-gap semiconductor mesoscopic film. From the outset, QDSSCs have been pushed to take advantage of the benefits of the quantum dots (QDs), including high absorption coefficient,[15,16] tunable band gap by size,[17,18] and possible multiple exciton generation,[19−21] to open a new avenue to clean and cost-efficient photovoltaics.[22] Despite their enormous potentiality, the performance of QDSSCs has still remained low after many years of effort.[23,24] Up to now, the highest power conversion efficiency (PCE) of QDSSC is 5.4%, achieved with Mn^{2+}-doped CdS and CdSe QDs anchored on TiO_2.[25] We have recently found that exquisite control over anchoring of the semiconductor QD layer on the mesoporous TiO_2 films is imperative to the photovoltaic performance but demands an extra effort.[26] ZnO is known to have better surface processability than TiO_2, and this has allowed vertically aligned ZnO nanorod arrays (NRs) based QDSSCs to achieve an efficiency of about 4.74%.[27] This photovoltaic efficiency is close to those of the TiO_2-based cells and is primarily ascribed to the impressive V_{oc} of about 0.85 V,[28] which is much higher than the typical V_{oc} values of 0.55−0.60 V with TiO_2.[29]

One of the problems for applying the vertically aligned ZnO NRs to solar cells is the difficulty in growing them longer than 10 μm with a diameter of less than 100 nm. Although ZnO nanowires of >40 μm length have been synthesized,[30] their diameters are correspondingly large, resulting in an overall decrease in the specific surface area. This is probably where ZnO nanotetrapods (TPs) can be put to good use in combination with the NRs because they can be easily assembled into a three-dimensional (3D) network structure with a thickness far over 10 μm. Such a 3D structure can be further processed to build a hierarchical branching framework to increase the surface area for better light harvesting. Moreover, conceivably, the interface between a NR layer and a TP layer is electrically as well as mechanically superior to that between a flat substrate and the TP layer simply because of the possible partial interpenetration between the two nanostructured layers.

The primary goal of the present work was to design and fabricate the double-layer structure of ZnO NRs and TPs, as shown in Scheme 1, and then to study the double-layer structure for QDDSCs. In order to improve the binding between FTO and the TP layer, a 2-μm-thick NR was employed as a buffer layer, the efficiency of ZnO NRs of which

Received: January 18, 2013
Accepted: April 25, 2013
Published: April 25, 2013

   dx.doi.org/10.1021/am400235g | ACS Appl. Mater. Interfaces 2013, 5, 4000−4005

Scheme 1. Layout of the Double-Layer-Assembly Branching Processes for Fabrication of the Branched ZnO Double-Layer NR−TP Film Photoanode

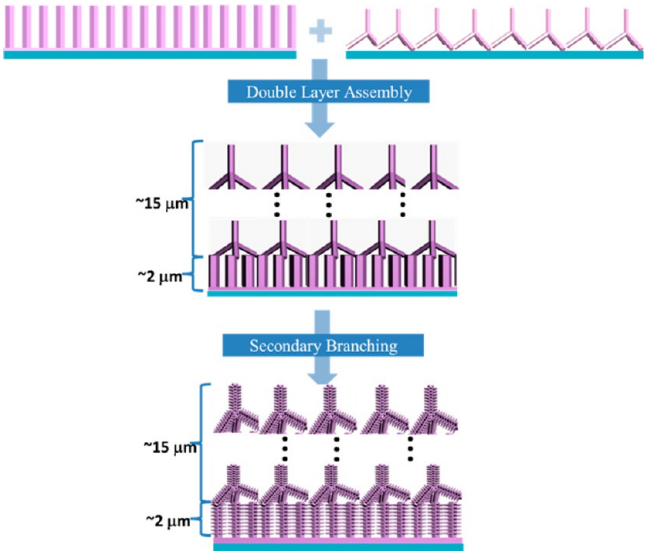

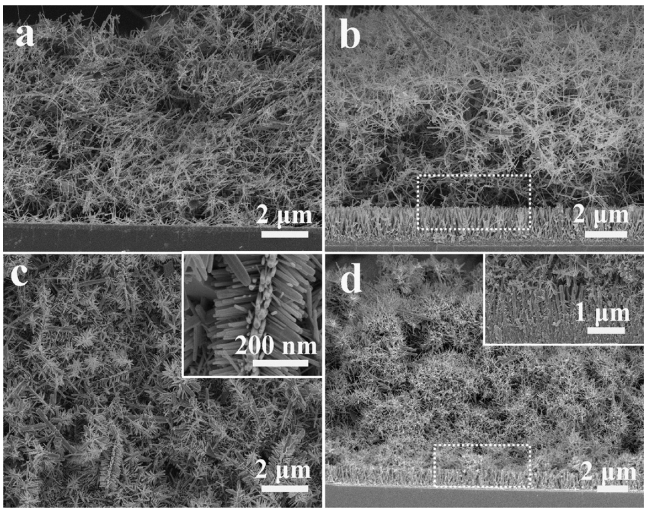

Figure 1. SEM images (cross-sectional view) of (a) single-layer ZnO TPs, (b) double-layer ZnO NR−TP films, and (d) branched double-layer ZnO NR−TP films. Insets: contact areas between the NR and TP layers. (c) Top section of branched double-layer ZnO NR−TP films. Inset: enlarged SEM image showing more details of a branched TP.

only is 1.12% (seen in Figure S3 and Table S1 of Supporting Information, SI) The QDSSC based on the double layer has attained 4.43% PCE, which is about a 30% enhancement compared to the single-TP-layer photoanode. Our dynamic transport study has revealed that this buffer layer could indeed block out the recombination and thereby improve the charge collection. Then both the NR and TP layers were subjected to secondary branching, which has previously proved effective in significantly enhancing the light harvesting for photoelectrochemical water splitting.[31] The secondary-branching strategy, in combination with the double-layer NR−TP strategy, has pushed the PCE further to above 5.24%, resulting from a better charge transport and less recombination, as informed from our dynamic transport study.

The ZnO TPs that we synthesized have four arms of about 100 nm in diameter and over 1 μm in length although vapor-transport grown.[32] Also, the ZnO NRs are vertically grown on FTO substrates in aqueous solution, and the individual nanorods have a mean diameter of ∼100 nm and a length of 1−2 μm.[33] With the doctor blade technique, ZnO TPs are deposited on the FTO with ZnO NRs to form a film, resulting in a double-layer architecture. A further elaboration on the double-layer architecture is to execute additional branching via solution-phase growth so as to improve the specific surface area and network connectivity. Figure 1 shows scanning electron microscopy (SEM) images of the photoanode structures used in our experiments, including a single-TP-layer film (cross-sectional view, a), a NR−NT double-layer film (cross-sectional view, b; top view, c), and a branched NR−NT double-layer film (cross-sectional view, d). Clearly, in both the single-TP-layer film (with a thickness of ∼15 μm) and double-layer film (with a total thickness of ∼17 μm: 15 μm TP plus 2 μm NR), the TPs are inextricably connected to each other. Additionally, in the double-layer structure, one can see that the TP arms tend to penetrate into the NR films (seen in Figure 1b), effectively enhancing the mechanical and electrical contact between them. Although the connectivity between the tetrapods is very good, there are still many void spaces (see Figure 1b) present in these films because of the open structure of the TPs. In order to remedy this problem, we have performed an additional branching step in this double-layer NR−TP structure. As shown in the inset of Figure 1c, after secondary growth, the ZnO branches can be clearly seen with lengths of 200−400 nm and diameters of 50−80 nm. The branched double-layer films are shown in Figure 1c,d, revealing that the void spaces have been evidently decreased and the connectivity among the TPs and NRs has been pronouncedly improved, accompanied by a slight increase (1−2 μm) of the overall thickness of the films. Thankfully, the seeded growth has formed a dense ZnO layer right at the interface between the FTO and the ZnO NR, as can be seen from the inset in Figure 1d, which turned out to be important in acting as an electron-transporting but hole-blocking layer for the photoanode. This double-layer film forms the basis of the key photoanode structure studied in this work. Diffuse-reflectance spectra of the single-layer ZnO NR and TP films, the double-layer ZnO NR−TP film, and the additionally branched, double-layer NR−TP film have been measured (see Figure S2 in the SI). The band-edge absorption at 380 nm (3.26 eV) is the common feature observed for the four ZnO films. However, by comparing the films of single-layer TPs, double-layer NR−TP, and branched NR−TP, one can see that the ZnOnonbranched NR−TP film exhibits smaller reflectance than the secondary branched NR−TP film in the wide-visible-wavelength region but somewhat large in the UV end. This can be explained by the lower density of the nonbranched films, which scatter light much more strongly in the short-wavelength region than in the long-wavelength region.

The mesoscopic ZnO films referred to above were then coated with a thin layer of CdSe/CdS throughout their thickness to sensitize solar cells. High-resolution SEM (HRSEM) images of the typical CdSe/CdS-sensitized ZnO TPs and branched TPs that we have fabricated are presented in Figure 2a,b. Here the small CdSe and CdS nanocrystals were grown on the TPs and branched TPs by the successive ionic layer adsorption and reaction process.[34,35] The inner CdS nanocrystal layer was formed by immersing the TP films into anionic S^{2-} and cationic Cd^{2+} solutions alternately for 2−3

dx.doi.org/10.1021/am400235g | ACS Appl. Mater. Interfaces 2013, 5, 4000−4005

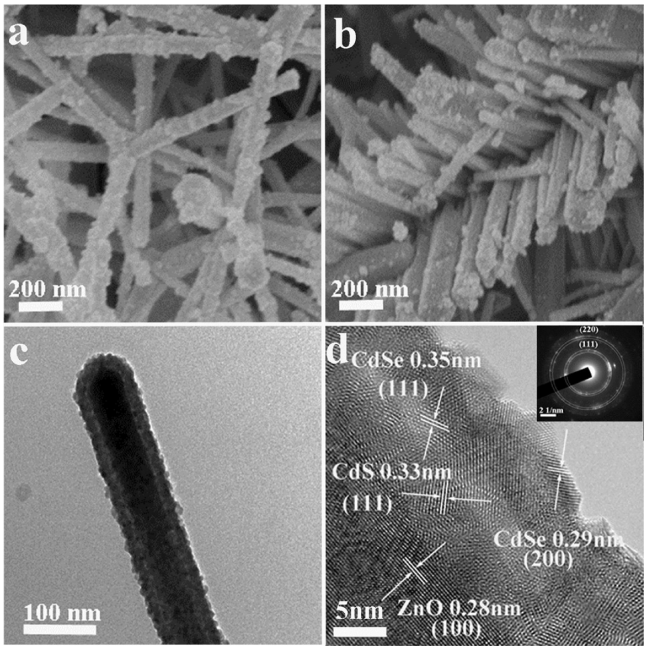

Figure 2. HRSEM images of (a) CdSe/CdS/ZnO TPs and (b) branched CdSe/CdS/ZnO TPs. (c) TEM image of a CdSe/CdS/ZnO TP. (d) HRTEM image of a CdSe/CdS/ZnO TP. Inset: electron diffraction pattern of the CdSe/CdS/ZnO TP.

cycles. Then the outer CdSe nanocrystal layer was similarly formed, by immersing the film into a NaHSe solution (by reducing Se powder with $NaBH_4$) and a cationic Cd^{2+} solution alternately for 4−5 cycles (for details see the Experimental Section in SI). Such a cosensitization scheme was used because the CdS- and CdSe-cosensitized ZnO TPs should have a broader absorbance range and thus a higher efficiency than single-semiconductor-sensitized solar cells. Indeed, that is what we observed, as will be presented below (for more details, see Figure S1 and Table S1 in the SI). Figure 2c shows a transmission electron microscopy (TEM) image of the CdSe/CdS/ZnO core/shell TP arm, which exhibits a mean thickness of 10 nm for the CdSe and CdS shells. Portrayed in Figure 2d is a high-resolution TEM (HRTEM) image of the CdS and CdSe nanocrystal layers. Clearly, the outer *d* spacing of the nanocrystals is measured to be 0.35 and 0.29 nm, which match well the interplanar spacing of the (111) and (200) planes of CdSe, while the interlayer *d* spacing of nanoparticles is 0.33 nm, assignable to the interplanar spacing of the (111) planes of the CdS. The inset in Figure 2d gives an electron diffraction pattern of the CdSe/CdS/ZnO TPs, which clearly indicates the presence of CdSe and CdS polycrystal alloys, with (220) and (111) planes. Together, we have established the well-defined structure of the branched double-layer photoanode film sensitized by a CdSe/CdS QD shell.

Figure 3a shows the UV-related performance of these three semiconductor-sensitized ZnO films. UV−vis absorption spectra have been recorded to examine the light-harvesting abilities of the QD-sensitized films (see the measurement method in the Experimental Section) and are collected in Figure 3a. All of the films have a similar absorption onset at around 720 nm, corresponding to a band gap of 1.72 eV. However, the absorbance of the branched CdSe/CdS/ZnO NR−TP film is apparently stronger than that of the other two films in the visible region from 400 to 700 nm. Such enhanced

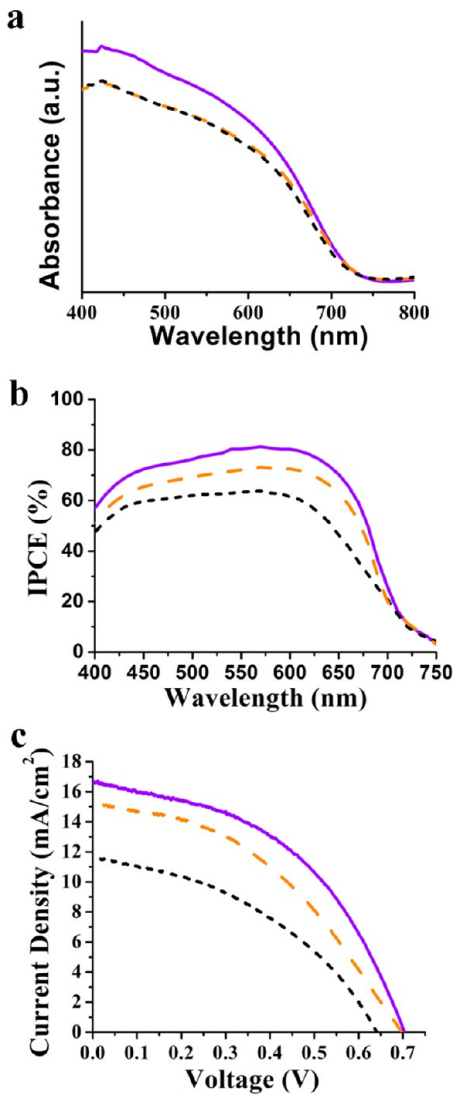

Figure 3. (a) UV−vis absorbance spectra, (b) IPCE curves, and (c) *J*−*V* curves (under illumination) of the CdSe/CdS/ZnO TP film (black short-dashed line), the CdSe/CdSe/ZnO NR−TP film (orange dashed line), and the branched CdSe/CdS/ZnO branched NR−TP film (violet solid line).

absorbance is believed to result from secondary branching, which allows more semiconductor nanocrystals to be loaded than with the two other films described above.

The incident photon-to-current conversion efficiencies (IPCEs) as a function of the light wavelengths are shown in Figure 3b. The single-layer CdSe/CdS/ZnO TP electrode exhibits a broad response with photocurrent onsets around 720 nm and a maximum IPCE of ∼62% at ∼520 nm. After insertion of a ZnO NR between the FTO and ZnO TP layers, a significant increase of the photocurrent response is observed from 500 to 700 nm, with the maximum IPCE of about 74% shifted to ∼580 nm. The overall IPCE enhancement highlights the importance of the branched and double-layer strategies in improving the light harvesting and charge collection. In particular, the remarkable increment in the 600−800 nm region of IPCE from the single-layer film to the double-layer film can be largely accounted for by the fact that the double-layer structure gains better charge collection by shortening the electron-transport time and increasing the electron lifetime,

dx.doi.org/10.1021/am400235g | ACS Appl. Mater. Interfaces 2013, 5, 4000−4005

which will be confirmed below (see Figures 4 and 5). Furthermore, a higher photocurrent response of the branched

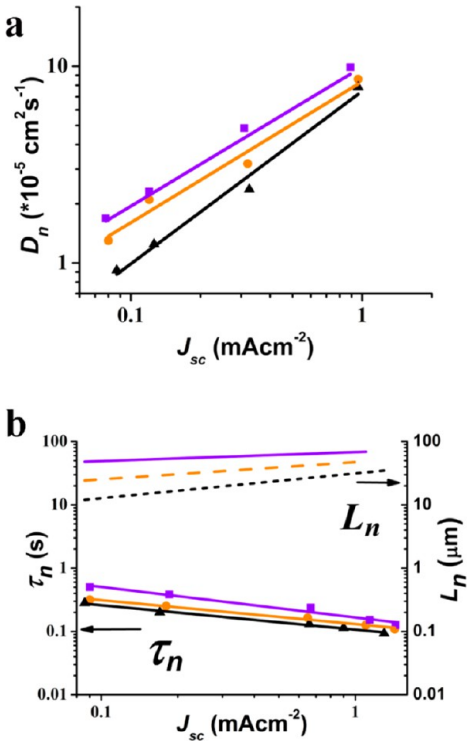

Figure 4. (a) Electron diffusion coefficients D_n and (b) electron lifetimes τ_n as a function of the short-circuit photocurrent (J_{sc}) for the CdSe/CdS/ZnO TPs film (black line + triangle symbol), the CdSe/CdSe/ZnO NR−TP film (orange line + circle symbol), and the branched CdSe/CdS/ZnO NR−TP film (violet line + square symbol). (b) Diffusion lengths L_n as a function of the short-circuit photocurrent (J_{sc}) for the CdSe/CdS/ZnO TP film (black short-dashed line), the CdSe/CdSe/ZnO NR−TP film (orange dashed line), and the branched CdSe/CdS/ZnO NR−TP film (violet solid line).

NR−TP film than the nonbranched NR−TP film has been observed in the visible-wavelength region, reaching the maximum 80% IPCE at ∼590 nm. This result conforms to the absorption intensity enhancement due to the branch growth, as seen in the UV−vis spectra.

The J−V curves under illumination of the three photoanodes are shown in Figure 3c. Table 1 summarizes the cell performance parameters, including the short-circuit current (J_{sc}), open-circuit voltage (V_{oc}), fill factor (FF), and PCE η. Especially noteworthy is an increase in V_{oc} for the NR−TP (0.696 V) and branched NR−TP (0.703 V) double-layer film photoanodes, compared with the single-layer TP film photoanode (∼0.64 V). Moreover, the double-layer design and secondary-branching growth have increased the photocurrent successively: J_{sc} ∼ 15.16 mA/cm^2 for the double-layer NR−TP film and J_{sc} ∼ 16.56 mA/cm^2 for the branched NR−TP film. The higher J_{sc} value of the branched NR−TP film is achieved because of the enhanced IPCE (Figure 4) in the long-wavelength region. The FFs are all over 0.4 for the single-layer TPs (0.43), NR−TP double-layer (0.42), and branched NR−TP double-layer (0.45) films when a Cu_2S brass electrode was employed as the counter electrode (see the Experimental Section in the SI). The highest overall PCE at 5.24% has been obtained with the branched NR−TP double-layer film photoanode. This significant PCE gain demonstrates that the

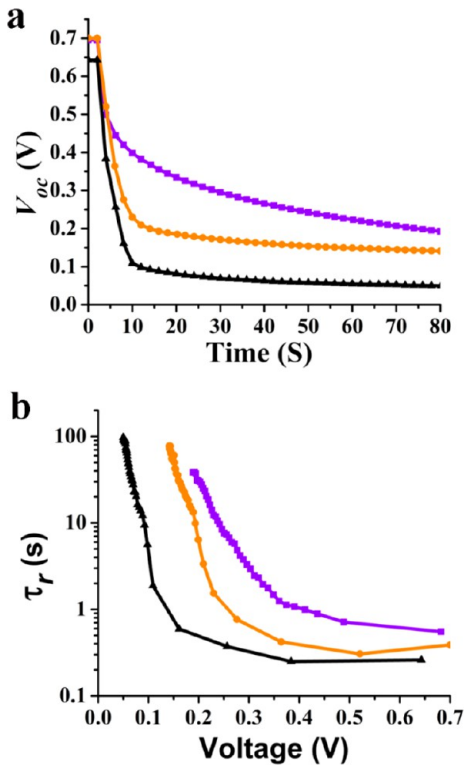

Figure 5. (a) Photovoltage decay and (b) electron lifetimes τ_r determined therefrom for the CdSe/CdS/ZnO TP film (black line + triangle symbol), the CdSe/CdSe/ZnO NR−TP film (orange line + circle symbol), and the branched CdSe/CdS/ZnO NR−TP film (violet line + square symbol).

Table 1. Performance Parameter Summary of the QDSSCs Based on the CdSe/CdS/ZnO TP, CdSe/CdS/ZnO NR−TP, and CdSe/CdS/ZnO Branched NR−TP Films

sample	J_{sc} (mA/cm^2)	V_{oc} (V)	FF	η (%)
CdSe/CdS/ZnO branched NR−TP film	16.56	0.703	0.45	5.24
CdSe/CdS/ZnO NR−TP film	15.16	0.696	0.42	4.43
CdSe/CdS/ZnO TP film	12.23	0.643	0.43	3.32

double-layer design and branching strategy are effective means for developing high-efficiency semiconductor-sensitized solar cells.

To understand the photovoltaic performance presented above, we have measured charge-transport and recombination properties of the two nonbranched solar cells based on the single-layer TP film and the double-layer NR−TP film and the branched solar cells based on the double-layer NR−TP film. To study the electron-transport dynamics, we employed intensity-modulated photocurrent spectroscopy under short-circuit conditions, while for the investigation of recombination, the electron lifetime was probed using intensity-modulated photovoltage spectroscopy (IMVS) under open-circuit conditions.[36−40] In these studies, a diode laser light source with variable intensities at 535 nm was used. The thickness of the single-layer TP photoanode is 15 ± 1.5 μm, resulting in an overall thickness of the nonbranched and branched NR−TP photoanodes being about 17 μm.

Figure 4a plots the obtained electron diffusion coefficient D_n as a function of the short-circuit photocurrent (J_{sc}, with D_n ≈

dx.doi.org/10.1021/am400235g | ACS Appl. Mater. Interfaces 2013, 5, 4000−4005

$d^2/C\tau_t$, where d is the thickness of the ZnO film, C is a constant with a value of about 2.35, and τ_t is electron transport time) for the photoanodes under study. One immediately sees that the branched double-layer NR−TP solar cell exhibits much higher D_n values than the two nonbranched ZnO solar cells. This significant improvement of electron transport can only be attributed to secondary branching. Understandably, as secondary branching proceeds, the framework should become more and more highly connected and dense, facilitating electron transport. As to the two nonbranched films, the D_n curve for the double-layer NR−TP photoanode is above that for the single-layer TP one. This presumably results from the better contacts between the ZnO NRs and FTO than between the TPs and FTO and the more directed electron transport in the NRs. It therefore proves that our double-layer design can ensure fast transport to the FTO substrate through the vertical NRs.

Shown in Figure 4b is the electron lifetime τ_n, obtained from the IMVS time constant, as a function of J_{sc}. The faster recombination observed at higher J_{sc} can be explained by the increased local concentration of injected electrons and polysulfide.[41] The first point to note is that the electron lifetime τ_n is generally higher for the double-layer NR−TP films than for the single-layer films, as can be seen in Figure 4b. In other words, the recombination is slower for the double-layer films than for the single-layer films. Moreover, the branched films, in general, have a longer electron lifetime τ_n than the nonbranched films. This result is parallel to the electron lifetime τ_r measurement using the open-circuit photovoltage method, which will be presented below together with more discussion about this point. Figure S4 in the SI shows that D_n and τ_n of the thin nanorod film are both lower than those of the branched double-layer structure, which means our special structure has better charge transport and lower recombination than the vertical aligned nanorod structure.

By combination of the charge-transport and recombination properties, the electron diffusion length L_n [$L_n \approx (D_n\tau_n)^{1/2}$] can be obtained, which represents the average distance that carriers can travel in the materials and is thus a more useful parameter.[42] The calculated electron diffusion lengths for the three photoanodes are shown in Figure 4b as a function of J_{sc}. Significantly, of all of the ZnO films studied, the longest L_n has been achieved for the branched double-layer NR−TP film because of its simultaneously high D_n and low τ_n. Such an extremely long L_n for the branched double-layer NR−TP film (50−70 μm) promises to boost the light-harvesting efficiency of QDSSCs by replacing the common nanoparticle films.

To further verify the electron recombination characteristics of the photoanode films obtained above by the IMVS method, we have taken another approach, namely, the open-circuit photovoltage decay.[43] Here the cell open-circuit photovoltage was monitored as function of the time starting from the illuminated steady-state equilibrium to the dark equilibrium. Also, because of the recombination of excess electrons, the open-circuit photovoltage would decay, providing information about the electron lifetime. Figure 5a shows the time profiles of V_{oc} for the various photoanode films. The most salient feature is a significantly slower photovoltage decay for the branched double-layer NR−TP film than the nonbranched counterparts, pointing to a lower recombination rate. In addition, the double-layer film has shown a longer decay rate than the single-layer one for the nonbranched structures. This result is in agreement with that obtained from IMVS. The electron lifetime τ_r can be calculated from the following equation:

$$\tau_r = -\frac{k_B T}{e}\left(\frac{dV_{oc}}{dt}\right)^{-1} \quad (1)$$

where k_B is the Boltzmann constant, T is the absolute temperature, e is the electron charge, and dV_{oc}/dt is the derivative of the open-circuit photovoltage transient. On the basis of eq 1, the electron lifetime extracted from the open-circuit photovoltage decay data is presented in Figure 5b as a function of the open-circuit photovoltage. Overall, an approximately exponential increase in the electron lifetime can be recognized with decreasing photovoltage. It is reassuring that the general trend of the electron lifetimes τ_n parallels that measured by IMVS. The much enhanced electron lifetime arising from the double-layer strategy is reasonably ascribed to the hindered back-recombination at the FTO because of compact coverage by the ZnO NRs. In the single-layer ZnO TP solar cells, the geometry of the ZnO TPs themselves dictates that the film they formed will expose large void areas of the FTO surface to the electrolyte. So, the accumulated electrons on the FTO from charge separation and injection may recombine with the holes in the electrolyte, which explains why the open-circuit photovoltage declines faster in this case. However, when the vertical NR was deposited on the FTO, the resulting less exposed FTO to the electrolyte slowed back-recombination. As for the branching-induced lifetime enhancement, one might consider it a consequence of a more complete coverage of the FTO surface with ZnO after branched growth, meaning a larger contact area between ZnO and FTO (see the image in the inset of Figure 1d). In the seed-mediated growth for secondary branching, ZnO could also be directly deposited on the FTO substrate. The more complete coverage of FTO with ZnO helps to block electron recombination. It is also not uncommon that leftover species such as polymers or surfactants introduced in the preparation solution could modify the surfaces of ZnO as well as the FTO, forming an ultrathin recombination−blocking layer.[44]

We have proposed a new ZnO photoanode design for QDSSCs, which is based on a double-layer architecture and a secondary branching scheme. This design has been implemented by the successfully fabrication of compact ZnO NRs on FTO, assembling a uniform ZnO TP layer on the array and growing additional ZnO branches to form a new branched ZnO NR−TP photoanode. This photoanode combines the advantages of a directed vertical electric transport of the ZnO NRs, an excellent network connectivity of the ZnO TPs, the good contacts between the ZnO NRs, FTO, and ZnO TPs, and the significantly enhanced light-harvesting and carrier dynamic properties arising from secondary branching. Those desirable properties have been translated to an improved performance of the corresponding QDSSCs. The maximum PCE has reached up to 5.24%, close to the record of QDSSCs. Although the FF and V_{oc} are still relatively low compared to those of DSSCs at this time, we believe that further improvement based on the ZnO nanostructure QDSSCs can be achieved by applying a new counter electrode and by designing new QD layer structures. Finally, the dynamic charge-transport measurements revealed reduced charge recombination and enhancement of charge transport by the branching double-layer structure. Our architectural design of the photoanode embodied by branched

double-layer ZnO NRs and TPs should facilitate the development of QDSSCs.

■ ASSOCIATED CONTENT

Supporting Information

Experimental section including material synthesis, characterization, and solar cell fabrication and measurement, UV−vis absorbance spectra and $J-V$ curves of different semiconductor-sensitized TP solar cells, diffuse-reflectance spectra of the NR, single TP, double-layer, and branched double-layer films, the $J-V$ curve, electron diffusion coefficient, and electron lifetime of the CdSe/CdS/ZnO NRs film, and table of parameters describing the performance of TP and NR films. This material is available free of charge via the Internet at http://pubs.acs.org.

■ AUTHOR INFORMATION

Corresponding Author

*Tel: 852-2358-7362. Fax: 852-2358-1594. E-mail: chsyang@ust.hk.

Notes

The authors declare no competing financial interest.

■ ACKNOWLEDGMENTS

This work was supported by the HK-RGC General Research Funds (Grants HKUST 606511, 605710, and 604809).

■ REFERENCES

(1) Bang, J. H.; Kamat, P. V. *ACS Nano* **2009**, *3*, 1467.
(2) Kamat, P. V.; Tvrdy, K.; Baker, D. R.; Radich, J. G. *Chem. Rev.* **2010**, *110*, 6664.
(3) Nozik, A. J.; Beard, M. C.; Luther, J. M.; Law, M.; Ellingson, R. J.; Johnson, J. C. *Chem. Rev.* **2010**, *110*, 6873.
(4) Nozik, A. J. *Physica E* **2002**, *14*, 115.
(5) Qi, X. P.; She, G. W.; Liu, Y. Y.; Mu, L. X.; Shi, W. S. *Chem. Commun.* **2012**, *48*, 242.
(6) Sun, W. T.; Yu, Y.; Pan, H. Y.; Gao, X. F.; Chen, Q.; Peng, L. M. *J. Am. Chem. Soc.* **2008**, *130*, 1124.
(7) Chang, C. H.; Lee, Y. L. *Appl. Phys. Lett.* **2007**, *91*, 053503.
(8) Leschkies, K. S.; Divakar, R.; Basu, J.; Enache-Pommer, E.; Boercker, J. E.; Carter, C. B.; Kortshagen, U. R.; Norris, D. J.; Aydil, E. S. *Nano Lett.* **2007**, *7*, 1793.
(9) Farrow, B.; Kamat, P. V. *J. Am. Chem. Soc.* **2009**, *131*, 11124.
(10) Lee, H.; Wang, M. K.; Chen, P.; Gamelin, D. R.; Zakeeruddin, S. M.; Gratzel, M.; Nazeeruddin, M. K. *Nano Lett.* **2009**, *9*, 4221.
(11) Hyun, B. R.; Zhong, Y. W.; Bartnik, A. C.; Sun, L. F.; Abruna, H. D.; Wise, F. W.; Goodreau, J. D.; Matthews, J. R.; Leslie, T. M.; Borrelli, N. F. *ACS Nano* **2008**, *2*, 2206.
(12) Girard, S. N.; He, J. Q.; Zhou, X. Y.; Shoemaker, D.; Jaworski, C. M.; Uher, C.; Dravid, V. P.; Heremans, J. P.; Kanatzidis, M. G. *J. Am. Chem. Soc.* **2011**, *133*, 16588.
(13) Lee, H.; Leventis, H. C.; Moon, S. J.; Chen, P.; Ito, S.; Haque, S. A.; Torres, T.; Nuesch, F.; Geiger, T.; Zakeeruddin, S. M.; Gratzel, M.; Nazeeruddin, M. K. *Adv. Funct. Mater.* **2009**, *19*, 2735.
(14) Guo, W.; Shen, Y. H.; Wu, M. X.; Wang, L.; Wang, L. L.; Ma, T. L. *Chem.—Eur. J.* **2012**, *18*, 7862.
(15) Yu, W. W.; Qu, L. H.; Guo, W. Z.; Peng, X. G. *Chem. Mater.* **2003**, *15*, 2854.
(16) Ovid'ko, I. A.; Sheinerman, A. G. *Phys. Rev. B* **2002**, *66*, 245309.
(17) Norris, D. J.; Efros, A. L.; Rosen, M.; Bawendi, M. G. *Phys. Rev. B* **1996**, *53*, 16347.
(18) Ruhle, S.; Shalom, M.; Zaban, A. *ChemPhysChem* **2010**, *11*, 2290.
(19) Ellingson, R. J.; Beard, M. C.; Johnson, J. C.; Yu, P. R.; Micic, O. I.; Nozik, A. J.; Shabaev, A.; Efros, A. L. *Nano Lett.* **2005**, *5*, 865.
(20) Nozik, A. J. *Chem. Phys. Lett.* **2008**, *457*, 3.
(21) Semonin, O. E.; Luther, J. M.; Choi, S.; Chen, H. Y.; Gao, J. B.; Nozik, A. J.; Beard, M. C. *Science* **2011**, *334*, 1530.
(22) Kramer, I. J.; Sargent, E. H. *ACS Nano* **2011**, *5*, 8506.
(23) Kamat, P. V. *Acc. Chem. Res.* **2012**, *45*, 1906.
(24) Kamat, P. V. *J. Phys. Chem. C* **2008**, *112*, 18737.
(25) Santra, P. K.; Kamat, P. V. *J. Am. Chem. Soc.* **2012**, *134*, 2508.
(26) Yan, K. Y.; Chen, W.; Yang, S. H. *J. Phys. Chem. C* **2013**, *117*, 92.
(27) Xu, J.; Yang, X.; Wang, H. K.; Chen, X.; Luan, C. Y.; Xu, Z. X.; Lu, Z. Z.; Roy, V. A. L.; Zhang, W. J.; Lee, C. S. *Nano Lett.* **2011**, *11*, 4138.
(28) Xu, J.; Yang, X.; Yang, Q. D.; Wong, T. L.; Lee, S. T.; Zhang, W. J.; Lee, C. S. *J. Mater. Chem.* **2012**, *22*, 13374.
(29) Toyoda, T.; Shen, Q. *J. Phys. Chem. Lett.* **2012**, *3*, 1885.
(30) Xu, C. K.; Wu, J. M.; Desai, U. V.; Gao, D. *J. Am. Chem. Soc.* **2011**, *133*, 8122.
(31) Qiu, Y. C.; Yan, K. Y.; Deng, H.; Yang, S. H. *Nano Lett.* **2012**, *12*, 407.
(32) Qiu, Y. F.; Yang, S. H. *Adv. Funct. Mater.* **2007**, *17*, 1345.
(33) Greene, L. E.; Yuhas, B. D.; Law, M.; Zitoun, D.; Yang, P. *Inorg. Chem.* **2006**, *45*, 7535.
(34) Lu, Z. Z.; Xu, J.; Xie, X.; Wang, H. K.; Wang, C. D.; Kwok, S. Y.; Wong, T. L.; Kwong, H. L.; Bello, I.; Lee, C. S.; Lee, S. T.; Zhang, W. J. *J. Phys. Chem. C* **2012**, *116*, 2656.
(35) Luan, C. Y.; Vaneski, A.; Susha, A. S.; Xu, X. Q.; Wang, H. E.; Chen, X.; Xu, J.; Zhang, W. J.; Lee, C. S.; Rogach, A. L.; Zapien, J. A. *Nanoscale Res. Lett.* **2011**, *6*, 340.
(36) Dloczik, L.; Ileperuma, O.; Lauermann, I.; Peter, L. M.; Ponomarev, E. A.; Redmond, G.; Shaw, N. J.; Uhlendorf, I. *J. Phys. Chem. B* **1997**, *101*, 10281.
(37) Fisher, A. C.; Peter, L. M.; Ponomarev, E. A.; Walker, A. B.; Wijayantha, K. G. U. *J. Phys. Chem. B* **2000**, *104*, 949.
(38) Huang, S. Y.; Schlichthorl, G.; Nozik, A. J.; Gratzel, M.; Frank, A. J. *J. Phys. Chem. B* **1997**, *101*, 2576.
(39) Schlichthorl, G.; Park, N. G.; Frank, A. J. *J. Phys. Chem. B* **1999**, *103*, 782.
(40) Bisquert, J.; Vikhrenko, V. S. *J. Phys. Chem. B* **2004**, *108*, 2313.
(41) Martinson, A. B. F.; McGarrah, J. E.; Parpia, M. O. K.; Hupp, J. T. *Phys. Chem. Chem. Phys.* **2006**, *8*, 4655.
(42) Anta, J. A.; Guillen, E.; Tena-Zaera, R. *J. Phys. Chem. C* **2012**, *116*, 11413.
(43) Zaban, A.; Greenshtein, M.; Bisquert, J. *ChemPhysChem* **2003**, *4*, 859.
(44) Quintana, M.; Edvinsson, T.; Hagfeldt, A.; Boschloo, G. *J. Phys. Chem. C* **2007**, *111*, 1035.